ARTICLE

doi:10.1038/nature10361

Crystal structure of the β_2 adrenergic receptor–Gs protein complex

Søren G. F. Rasmussen[1,2]*, Brian T. DeVree[3]*, Yaozhong Zou[1], Andrew C. Kruse[1], Ka Young Chung[1], Tong Sun Kobilka[1], Foon Sun Thian[1], Pil Seok Chae[4], Els Pardon[5,6], Diane Calinski[3], Jesper M. Mathiesen[1], Syed T. A. Shah[7], Joseph A. Lyons[7], Martin Caffrey[7], Samuel H. Gellman[4], Jan Steyaert[5,6], Georgios Skiniotis[8], William I. Weis[1,9], Roger K. Sunahara[3] & Brian K. Kobilka[1]

G protein–coupled receptors (GPCRs) are responsible for the majority of cellular responses to hormones and neurotransmitters as well as the senses of sight, olfaction and taste. The paradigm of GPCR signalling is the activation of a heterotrimeric GTP binding protein (G protein) by an agonist–occupied receptor. The β_2 adrenergic receptor (β_2AR) activation of Gs, the stimulatory G protein for adenylyl cyclase, has long been a model system for GPCR signalling. Here we present the crystal structure of the active state ternary complex composed of agonist–occupied monomeric β_2AR and nucleotide–free Gs heterotrimer. The principal interactions between the β_2AR and Gs involve the amino– and carboxy–terminal α–helices of Gs, with conformational changes propagating to the nucleotide–binding pocket. The largest conformational changes in the β_2AR include a 14 Å outward movement at the cytoplasmic end of transmembrane segment 6 (TM6) and an α–helical extension of the cytoplasmic end of TM5. The most surprising observation is a major displacement of the α–helical domain of Gαs relative to the Ras–like GTPase domain. This crystal structure represents the first high–resolution view of transmembrane signalling by a GPCR.

Introduction

The β_2 adrenergic receptor (β_2AR) has been a model system for the large and diverse family of G protein-coupled receptors (GPCRs) for over 40 years. It was one of the first GPCRs to be characterized by radioligand binding, and it was the first neurotransmitter receptor to be cloned[1] and structurally determined by crystallography[2,3]. The β_2AR was initially identified based on its physiological and pharmacological properties, but it was not known if receptors and G proteins were separate entities, or parts of the same protein[4]. Subsequent biochemical studies led to the isolation and purification of functional β_2AR and Gs, the stimulatory G protein that activates adenylyl cyclase, and the reconstitution of this signalling complex in phospholipid vesicles[5,6]. The cooperative interactions of β_2AR and Gs observed in ligand binding assays formed the foundation of the ternary complex model of GPCR activation[7,8]. In the ternary complex consisting of agonist, receptor and G protein, the affinity of the receptor for agonist is enhanced and the specificity of the G protein for guanine nucleotides changes in favour of GTP over GDP. The GPCR field has evolved markedly since these initial studies. Isolation of the genes and cDNAs for the β_2AR and other GPCRs using protein sequencing and expression cloning led to the expansion of the family by homology cloning. More recently, sequencing of the human genome led to the identification of over 800 GPCR genes[9]. Experimental tools for identifying protein–protein interactions and for expression and silencing of genes have revealed a complex network of cellular signalling and regulatory pathways including G protein-independent activation of cytosolic kinases[10,11]. Nevertheless, the β_2AR continues to be a relevant model for most aspects of GPCR pharmacology, signalling and regulation.

Notwithstanding the remarkable advances in this field, we still know relatively little about the structural basis for transmembrane signalling by GPCRs. Figure 1 shows the G protein cycle for the β_2AR–Gs complex. Agonist binding to the β_2AR promotes interactions with GDP-bound Gsαβγ heterotrimer, leading to the exchange of GDP for GTP, and the functional dissociation of Gs into Gα-GTP and Gβγ subunits. The separate Gα-GTP and Gβγ subunits can modulate the activity of different cellular effectors (channels, kinases or other enzymes). The intrinsic GTPase activity of Gαs leads to hydrolysis of GTP to GDP and the reassociation of Gα-GDP and Gβγ subunits, and the termination of signalling. The active state of a GPCR can be defined as that conformation that couples to and stabilizes a nucleotide-free G protein. In this agonist-β_2AR–Gs ternary complex, Gs has a higher affinity for GTP than GDP, and the β_2AR has an approximately 100-fold higher affinity for agonists than does β_2AR alone. In an effort to understand the structural basis for GPCR signalling, we crystallized the β_2AR–Gs complex.

Crystallization of the β_2AR–Gs complex

The first challenge for crystallogenesis was to prepare a stable β_2AR–Gs complex in detergent solution. The β_2AR and Gs couple efficiently in lipid bilayers, but not in detergents used to solubilize and purify these proteins. We found that a relatively stable β_2AR–Gs complex could be prepared by mixing purified GDP-Gs (approximately 100 μM final concentration) with a molar excess of purified β_2AR bound to a high affinity agonist (BI-167107, Boehringer Ingelheim)[12] in dodecylmaltoside solution. Apyrase, a non-selective purine pyrophosphatase, was added to hydrolyse GDP released from Gs on forming a complex with the β_2AR. Removal of GDP was essential because both GDP and GTP

[1]Department of Molecular and Cellular Physiology, Stanford University School of Medicine, Stanford, California 94305, USA. [2]Department of Neuroscience and Pharmacology, The Panum Institute, University of Copenhagen, 2200 Copenhagen N, Denmark. [3]Department of Pharmacology, University of Michigan Medical School, Ann Arbor, Michigan 48109, USA. [4]Department of Chemistry, University of Wisconsin, Madison, Wisconsin 53706, USA. [5]Department of Molecular and Cellular Interactions, Vlaams Instituut voor Biotechnologie (VIB), Vrije Universiteit Brussel, B-1050 Brussel, Belgium. [6]Structural Biology Brussels, Vrije Universiteit Brussel, B-1050 Brussels, Belgium. [7]Membrane Structural and Functional Biology Group, Schools of Medicine and Biochemistry & Immunology, Trinity College, Dublin 2, Ireland. [8]Life Sciences Institute and Department of Biological Chemistry, University of Michigan, Ann Arbor, Michigan 48109, USA. [9]Department of Structural Biology, Stanford University School of Medicine, Stanford, California 94305, USA.
*These authors contributed equally to this work.

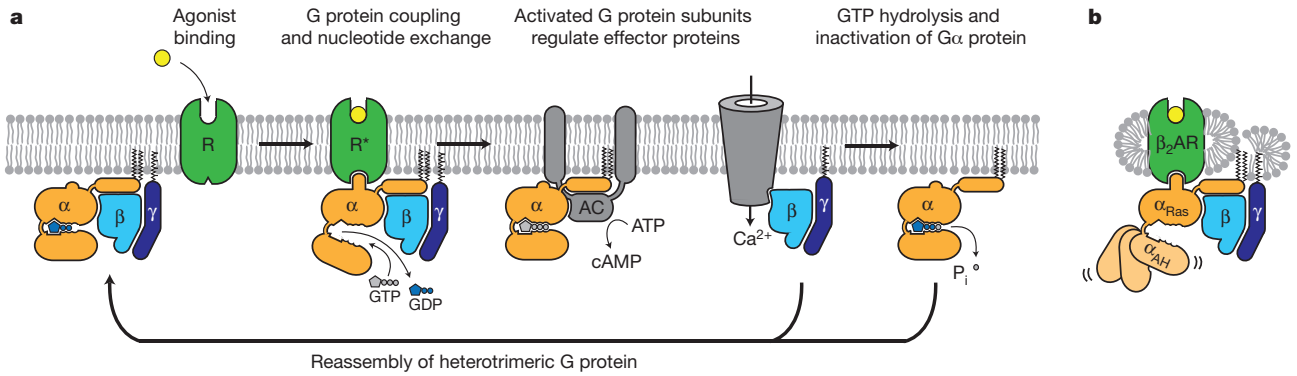

Figure 1 | G protein cycle for the β_2AR–Gs complex. **a**, Extracellular agonist binding to the β_2AR leads to conformational rearrangements of the cytoplasmic ends of transmembrane segments that enable the Gs heterotrimer (α, β, and γ) to bind the receptor. GDP is released from the α subunit upon formation of β_2AR–Gs complex. The GTP binds to the nucleotide-free α subunit resulting in dissociation of the α and βγ subunits from the receptor. The subunits regulate their respective effector proteins adenylyl cyclase (AC) and Ca^{2+} channels. The Gs heterotrimer reassembles from α and βγ subunits following hydrolysis of GTP to GDP in the α subunit. **b**, The purified nucleotide-free β_2AR–Gs protein complex maintained in detergent micelles. The Gαs subunit consists of two domains, the Ras domain (αRas) and the α-helical domain (αAH). Both are involved in nucleotide binding. In the nucleotide-free state, the αAH domain has a variable position relative the αRas domain.

can disrupt the high-affinity interaction between β_2AR and Gs (Supplementary Fig. 1a). The complex was subsequently purified by sequential antibody affinity chromatography and size-exclusion chromatography. The stability of the complex was enhanced by exchanging it into a recently developed maltose neopentyl glycol detergent MNG-3 (NG310, Anatrace)[13]. The complex could be incubated at room temperature for 24 h without any noticeable degradation; however, initial efforts to crystallize the complex using sparse matrix screens in detergent micelles, bicelles and lipidic cubic phase (LCP) failed.

To further assess the quality of the complex, we analysed the protein by single particle electron microscopy[34]. The results confirmed that the complex was monodisperse, but revealed two potential problems for obtaining diffraction of quality crystals. First, the detergent used to stabilize the complex formed a large micelle, leaving little polar surface on the extracellular side of the β_2AR–Gs complex for the formation of crystal lattice contacts. Our initial approach to this problem, which was to generate antibodies to the extracellular surface, was not successful. As an alternative approach, we replaced the unstructured amino terminus of the β_2AR with T4 lysozyme (T4L). We previously used T4L to facilitate crystallogenesis of the inactive β_2AR by inserting T4L between the cytoplasmic ends of TM5 and TM6 (ref. 3). Several different amino-terminal fusion proteins were prepared and single particle electron microscopy was used to identify a fusion with a relatively fixed orientation of T4L in relation to the β_2AR.

The second problem revealed by single particle electron microscopy analysis was increased variability in the positioning of the α-helical component of the Gαs subunit. Gαs consists of two domains, the Ras-like GTPase domain (GαsRas), which interacts with the β_2AR and the Gβ subunit, and the α-helical domain (GαsAH)[14]. The interface of the two Gαs subdomains forms the nucleotide-binding pocket (Fig. 1), and electron microscopy two-dimensional (2D) averages and three-dimensional (3D) reconstructions show that in the absence of guanine nucleotide, GαsAH has a variable position relative to the complex of T4L–β_2AR–GαsRas–Gβγ (Fig. 1b)[34].

We attributed the variable position of GαsAH to the empty nucleotide-binding pocket. However, as noted above both GDP and non-hydrolysable GTP analogues disrupt the β_2AR–Gs complex (Supplementary Fig. 1). The addition of the pyrophosphate analogue phosphonoformate (foscarnet) led to a significant increase in stabilization of GαsAH as determined by electron microscopy analysis of the detergent-solubilized complex[34]. Crystallization trials were carried out in LCP using a modified monolein (7.7 MAG, see Methods) designed to accommodate the large hydrophilic component of the T4L–β_2AR–Gs complex[15]. Although we were able to obtain small crystals that diffracted to 7 Å, we were unable to improve their quality through the use of additives and other modifications.

In an effort to generate an antibody that would further stabilize the complex and facilitate crystallogenesis, we crosslinked β_2AR and the Gs heterotrimer with a small, homobifunctional amine-reactive crosslinker and used this stabilized complex to immunize llamas. Llamas and other camelids produce antibodies devoid of light chains. The single domain antigen binding fragments of these heavy-chain-only antibodies, known as nanobodies, are small (15 kDa), rigid, and are easily cloned and expressed in *Escherichia coli* (Methods)[16]. We obtained a nanobody (Nb35) that binds to the complex and prevents dissociation of the complex by GTPγS (Supplementary Fig. 1). The T4L–β_2AR–Gs–Nb35 complex was used to obtain crystals that grew to 250 μm (Supplementary Fig. 2) in LCP (7.7 MAG) and diffracted to 2.9 Å. A 3.2 Å data set was obtained from 20 crystals and the structure was determined by molecular replacement (Methods).

The β_2AR–Gs complex crystallized in primitive monoclinic space group $P2_1$, with a single complex in each asymmetric unit. Figure 2a shows the crystallographic packing interactions. Complexes are arrayed in alternating aqueous and lipidic layers with lattice contacts formed almost exclusively between soluble components of the complex, leaving receptor molecules suspended between G protein layers and widely separated from one another in the plane of the membrane. Extensive lattice contacts are formed among all the soluble proteins, probably accounting for the strong overall diffraction and remarkably clear electron density for the G protein. Nb35 and T4L facilitated crystal formation. Nb35 packs at the interface of the Gβ and Gα subunits, with the complementarity determining region (CDR) 1 interacting primarily with Gβ and a long CDR3 loop interacting with both Gβ and Gα subunits. The framework regions of Nb35 from one complex also interact with Gα subunits from two adjacent complexes. T4L is linked to the β_2AR only through amino-terminal fusion, but packs against the amino terminus of the Gβ subunit of one complex, the carboxy terminus of the Gγ subunit of another complex, and the Gα subunit of yet another complex. Figure 2b shows the structure of the complete complex including T4L and Nb35, and Fig. 2c shows the β_2AR–Gs complex alone.

Structure of the active-state β_2AR

The β_2AR–Gs structure provides the first high-resolution insight into the mechanism of signal transduction across the plasma membrane by a GPCR, and the structural basis for the functional properties of the ternary complex. Figure 3a compares the structures of the agonist-bound receptor in the β_2AR–Gs complex and the inactive

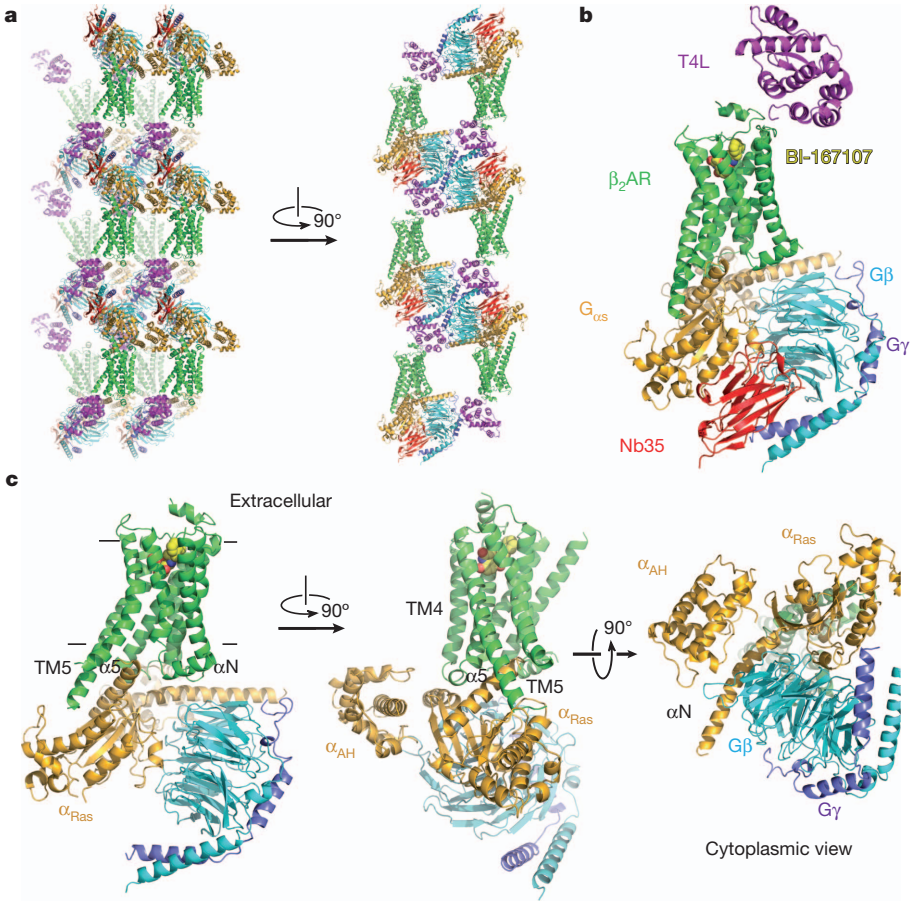

Figure 2 | Overall structure of the β_2AR–Gs complex. **a**, Lattice packing of the complex shows alternating layers of receptor and G protein within the crystal. Abundant contacts are formed among proteins within the aqueous layers. **b**, The overall structure of the asymmetric unit contents shows the β_2AR (green) bound to an agonist (yellow spheres) and engaged in extensive interactions with Gαs (orange). Gαs together with Gβ (cyan) and Gγ (purple) constitute the heterotrimeric G protein Gs. A Gs-binding nanobody (red) binds the G protein between the α and β subunits. The nanobody (Nb35) facilitates crystallization, as does T4 lysozyme (magenta) fused to the amino terminus of the β_2AR. **c**, The biological complex omitting crystallization aids, showing its location and orientation within a cell membrane.

carazolol-bound β_2AR. The largest difference between the inactive and active structures is a 14 Å outward movement of TM6 when measured at the Cα carbon of E268. There is a smaller outward movement and extension of the cytoplasmic end of the TM5 helix by 7 residues. A stretch of 26 amino acids in the third intracellular loop (ICL3) is disordered. Another notable difference between inactive and active structures is the second intracellular loop (ICL2), which forms an extended loop in the inactive β_2AR structure and an α-helix in the β_2AR–Gs complex. This helix is also observed in the β_2AR–Nb80 structure (Fig. 3b); however, it may not be a feature that is unique to the active state, because it is also observed in the inactive structure of the highly homologous avian β_1AR (ref. 17).

The quality of the electron density maps for the β_2AR is highest at the β_2AR–GαsRas interface, and much weaker for the extracellular half. The extracellular half of the receptor is not stabilized by any packing interactions either laterally with adjacent receptors in the membrane or through the extracellular surface. Instead, the extracellular region is indirectly tethered to the well-packed soluble components by the amino-terminal fusion to T4 lysozyme (Fig. 2a). Given the flexible and dynamic nature of GPCRs, the absence of stabilizing packing interactions may lead to structural heterogeneity in the extracellular half of the receptor and, consequently, to the limited quality of the electron density maps. However, the overall structure of the β_2AR in the T4L–β_2AR–Gs complex is very similar to our recent active-state structure of β_2AR stabilized by a G protein mimetic nanobody (Nb80)[12]. In the β_2AR–Nb80 crystal, each receptor molecule has extensive packing interactions with adjacent receptors and the quality of the electron density maps for the agonist-bound β_2AR in this complex is remarkably good for a 3.5 Å structure. Therefore, the β_2AR–Nb80 structure allows us to confidently model BI-167107 here, and provide a more reliable view of the conformational rearrangements of amino acids around the ligand-binding pocket and between the ligand-binding pocket and the Gs-coupling interface[12].

The overall root mean square deviation between the β_2AR components in the β_2AR–Gs and β_2AR–Nb80 structures is approximately 0.6 Å, and they differ most at the cytoplasmic ends of transmembrane helices 5 and 6 where they interact with the different proteins (Fig. 3b–d). The largest divergence is a 3 Å outward movement at the end of helix 6 in the β_2AR–Gs complex. However, the differences between these two structures are very small at the level of the most highly conserved amino acids (E/DRY and NPxxY), which are located at the cytoplasmic ends of the transmembrane segments (Fig. 3c, d). These conserved sequences have been proposed to be important for activation or for maintaining the receptor in the inactive state[18]. Of these residues, only Arg 131 differs significantly between these two structures. In β_2AR–Nb80 Arg 131 interacts with Nb80, whereas in the β_2AR–Gs structure Arg 131 packs against Tyr 391 of Gαs (Supplementary Fig. 3). The high structural similarity is in agreement with the functional similarity of these two proteins. The β_2AR–Nb80 complex shows the same high affinity for the agonist isoproterenol as does the β_2AR–Gs complex[12], consistent with high structural homology around the ligand binding pocket.

The active state of the β_2AR is stabilized by extensive interactions with GαsRas (Fig. 4). There are no direct interactions with Gβ or Gγ subunits. The total buried surface of the β_2AR–GαsRas interface is 2,576 Å^2 (1,300 Å^2 for GαsRas and 1,276 Å^2 for the β_2AR). This interface is formed by ICL2, TM5 and TM6 of the β_2AR, and by α5-helix, the αN–β1 junction, the top of the β3-strand, and the α4-helix of GαsRas (see Supplementary Table 1 for specific interactions). Some of the β_2AR sequences involved in this interaction have been shown to have a role in G protein coupling; however, there is no clear consensus sequence for Gs-coupling specificity when these segments are aligned with other GPCRs. Perhaps this is not surprising considering that the β_2AR also couples to Gi and that many GPCRs couple to more than one G protein isoform. Of the 21 amino acids of Gs that are within 4 Å of the β_2AR, only five are identical between Gs and Gi, and all of these

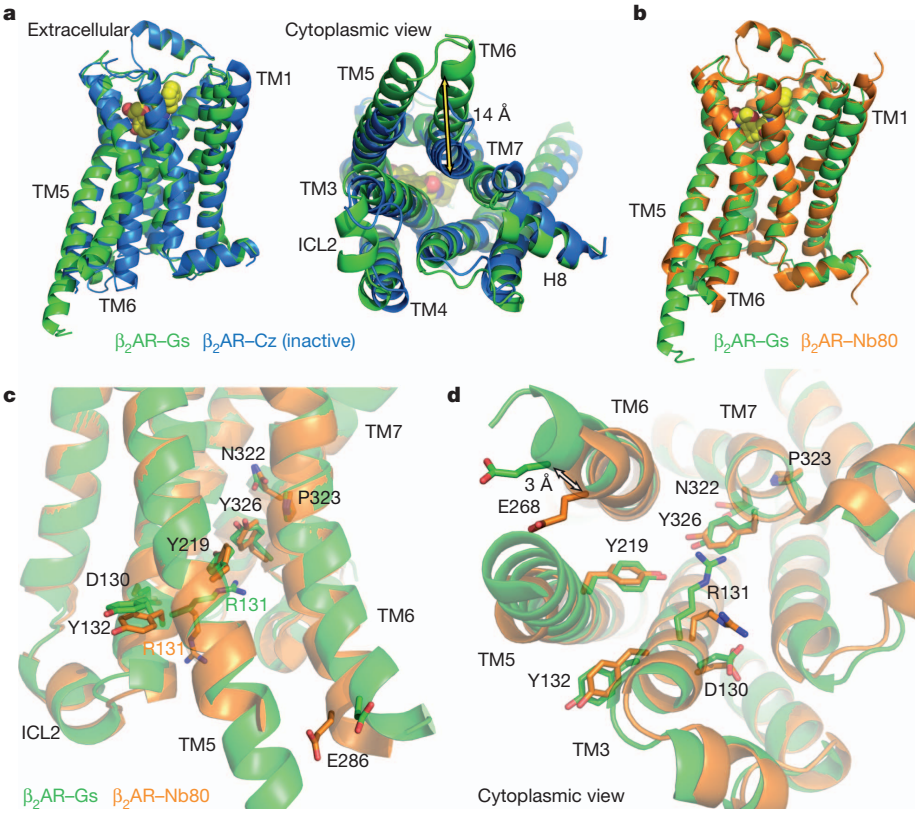

Figure 3 | Comparison of active and inactive β_2AR structures. **a**, Side and cytoplasmic views of the β_2AR–Gs structure (green) compared to the inactive carazolol-bound β_2AR structure[3] (blue). Significant structural changes are seen for the intracellular domains of TM5 and TM6. TM5 is extended by two helical turns whereas TM6 is moved outward by 14 Å as measured at the α-carbons of Glu 268 (yellow arrow) in the two structures. **b**, β_2AR–Gs compared with the nanobody-stabilized active state β_2AR–Nb80 structure[12] (orange). **c**, The positions of residues in the E/DRY and NPxxY motifs and other key residues of the β_2AR–Gs and β_2AR–Nb80 structures. All residues occupy very similar positions except Arg 131 which in the β_2AR–Nb80 structure interacts with the nanobody. **d**, View from the cytoplasmic side of residues shown in **c**.

are in the carboxy-terminal α helix. The structural basis for G protein coupling specificity must therefore involve more subtle features of the secondary and tertiary structure. Nevertheless, a noteworthy interaction involves Phe 139, which is located at the beginning of the ICL2 helix and sits in a hydrophobic pocket formed by Gαs His 41 at the beginning of the β1-strand, Val 217 at the start of the β3-strand and Phe 376, Cys 379, Arg 380 and Ile 383 in the α5-helix (Fig. 4c). The β_2AR mutant F139A has severely impaired coupling to Gs[19]. The residue corresponding to Phe 139 is a Phe or Leu on almost all Gs coupled receptors, but is more variable in GPCRs known to couple to other G proteins. Of interest, the ICL2 helix is stabilized by an interaction between Asp 130 of the conserved DRY sequence and Tyr 141 in the middle of the ICL2 helix (Fig. 4c). Tyr 141 has been shown to be a substrate for the insulin receptor tyrosine kinase[20]; however, the functional significance of this phosphorylation is currently unknown.

The lack of direct interactions between the β_2AR and Gβγ is somewhat unexpected given that a heterotrimer is required for efficient coupling to a GPCR. Whereas Gβ does not interact directly with the β_2AR, it has an indirect but important role in coupling by stabilizing the amino-terminal α helix of Gαs (Fig. 2c). Several models involving GPCR dimers propose that one of the protomers interacts predominantly with Gα while the other interacts with Gβγ[21–23]. Consistent with these models, biochemical and biophysical evidence suggests that Gαi2 forms a stable complex with a LTB4 receptor dimer[24].

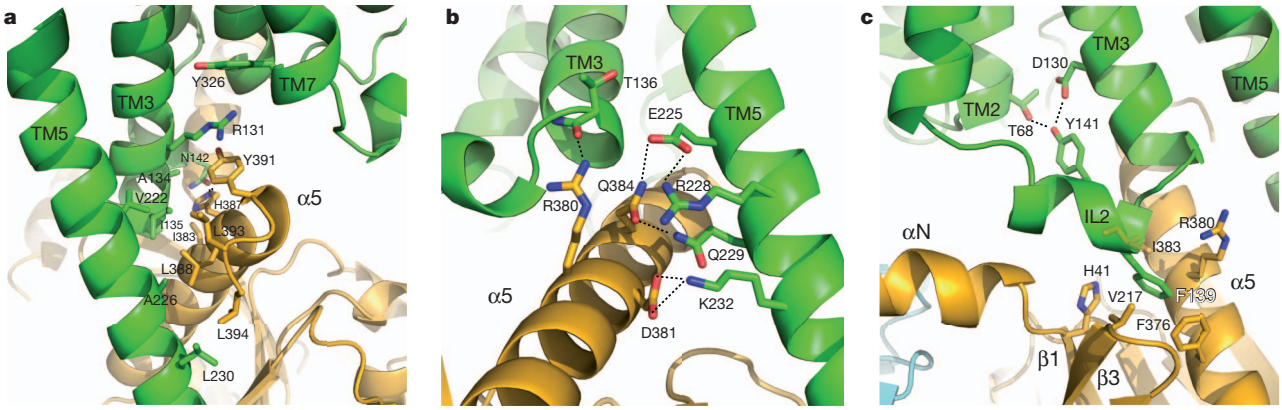

Figure 4 | Receptor-G protein interactions. **a**, **b**, The α5-helix of Gαs docks into a cavity formed on the intracellular side of the receptor by the opening of transmembrane helices 5 and 6. **a**, Within the transmembrane core, the interactions are primarily non-polar. An exception involves packing of Tyr 391 of the α5-helix against Arg 131 of the conserved DRY sequence in TM3 (see also Supplementary Fig. 3). Arg 131 also packs against Tyr 326 of the conserved NPxxY sequence in TM7. **b**, As α5-helix exits the receptor it forms a network of polar interactions with TM5 and TM3. **c**, Receptor residues Thr 68 and Asp 130 interact with the ICL2 helix of the β_2AR via Tyr 141, positioning the helix so that Phe 139 of the receptor docks into a hydrophobic pocket on the G protein surface, thereby structurally linking receptor–G protein interactions with the highly conserved DRY motif of the β_2AR.

Whereas the β_2AR efficiently activates Gs as a monomer, extensive biochemical and biophysical evidence supports the existence of β_2AR dimers or oligomers in living cells[25]. Therefore, we cannot exclude the possibility that in cell membranes one protomer of a β_2AR dimer may interact with the G$\beta\gamma$ subunit.

Structure of activated Gs

The most surprising observation in the β_2AR–Gs complex is the large displacement of the GαsAH relative to GαsRas (an approximately 127° rotation about the junction between the domains) (Fig. 5a). GαsAH moves as a rigid body as shown by the alignment of β_2AR–Gs with GαsAH from the crystal structure of Gαs–GTPγS[26] (Supplementary Fig. 4). In the structure of Gαs–GTPγS, the nucleotide-binding pocket is formed by the interface between GαsRas and GαsAH. Guanine nucleotide binding stabilizes the interaction between these two domains. The loss of this stabilizing effect of guanine nucleotide binding is consistent with the high flexibility observed for GαsAH in single particle electron microscopy analysis of the detergent-solubilized complex[34]. It is also in agreement with the increase in deuterium exchange at the interface between these two domains upon formation of the complex[35]. Recently double electron-electron resonance (DEER) spectroscopy was used to document large (up to 20 Å) changes in distance between nitroxide probes positioned on the Ras and α-helical domains of Gi upon formation of a complex with light-activated rhodopsin[27]. Finally, it has been shown that GαsRas and GαsAH can form a functional GTPase when expressed together as separate proteins[28]. Therefore, it is perhaps not surprising that GαsAH is displaced relative to GαsRas; however, its location in this crystal structure most probably reflects only one of an ensemble of conformations that it can adopt under physiological conditions, but has been stabilized by crystal packing interactions (Supplementary Fig. 5).

A potential concern is that Nb35, which was used to facilitate crystallogenesis, may be responsible for the displacement of the GαsAH. However, Nb35, which binds at the interface between Gβ and GαsRas (Fig. 2b and Supplementary Fig. 6), would not be expected to interact with the GαsAH or interfere with its interactions with GαsRas. None of the Nb35 contacts on the Ras domain are involved in interactions with GαsAH on the basis of the crystal structure of Gαs–GTPγS (1AZT). Moreover, if we superimpose the structures of the Ras domains of Gαs–GTPγS (1AZT) and β_2AR–Gs, there is no overlap between Nb35 and the α-helical domain of Gαs–GTPγS (Supplementary Fig. 6). Similarly, if we align the Gβ subunits of the Gi-GDP heterotrimer (1GP2) with that of β_2AR–Gs, there is no overlap between Nb35 and the α-helical domain of Gi (Supplementary Fig. 6). This analysis is in agreement with single particle electron microscopy studies which provide further evidence that Nb35 does not disrupt interactions between GαsAH and GαsRas[34].

The conformational links between the β_2AR and the nucleotide-binding pocket primarily involve the amino- and carboxy-terminal helices of Gαs (Fig. 4). Figure 5b focuses on the region of GαsRas that undergoes the largest conformational change when comparing the structure of GαsRas from the β_2AR–Gs complex with that from the Gαs–GTPγS complex[26]. The largest difference is observed for the α5-helix, which is displaced 6 Å towards the receptor and rotated as the carboxy-terminal end projects into transmembrane core of the β_2AR. Previous studies using a variety of approaches have demonstrated the important role of the α5-helix in GPCR–G protein interactions[29,30]. Associated with movement of the α5-helix, the β6-α5 loop, which interacts with the guanine ring in the Gαs–GTPγS structure, is displaced outward, away from the nucleotide-binding pocket (Fig. 5b–d). The movement of the α5-helix is also associated with changes in interactions between this helix and the β6-strand, the αN-β1 loop, and the α1-helix. The β1-strand forms another link between the β_2AR and the nucleotide-binding pocket. The carboxy-terminal end of this strand changes conformation around Gly 47, and there are further changes in the β1-α1 loop (P-loop) that coordinates the β-phosphate in the GDP and GTP-bound forms (Fig. 5b–d). The observations in the crystal structure are in agreement with deuterium exchange experiments where there is enhanced deuterium exchange in the β1-strand and the amino-terminal end of the α5-helix upon formation of the nucleotide-free β_2AR–Gs complex[35]. The deuterium exchange-mass spectrometry (DXMS) studies provide additional insights into the dynamic nature of these conformational changes in Gs upon complex formation[35].

The structure of a GDP-bound Gs heterotrimer has not been determined, so it is not possible to directly compare the Gαs–G$\beta\gamma$ interface before and after formation of the β_2AR–Gs complex. On the basis of the structure of the GDP-bound Gi heterotrimer[31], we do not observe large changes in interactions between GαsRas and G$\beta\gamma$ upon formation of the complex with β_2AR. This is also consistent with deuterium exchange studies[35]. As discussed above, Nb35 binds at the interface between GαsRas and Gβ (Fig. 2b); therefore, we cannot exclude the possibility that Nb35 may influence the relative orientation of the GαsRas–G$\beta\gamma$ interface in the crystal structure.

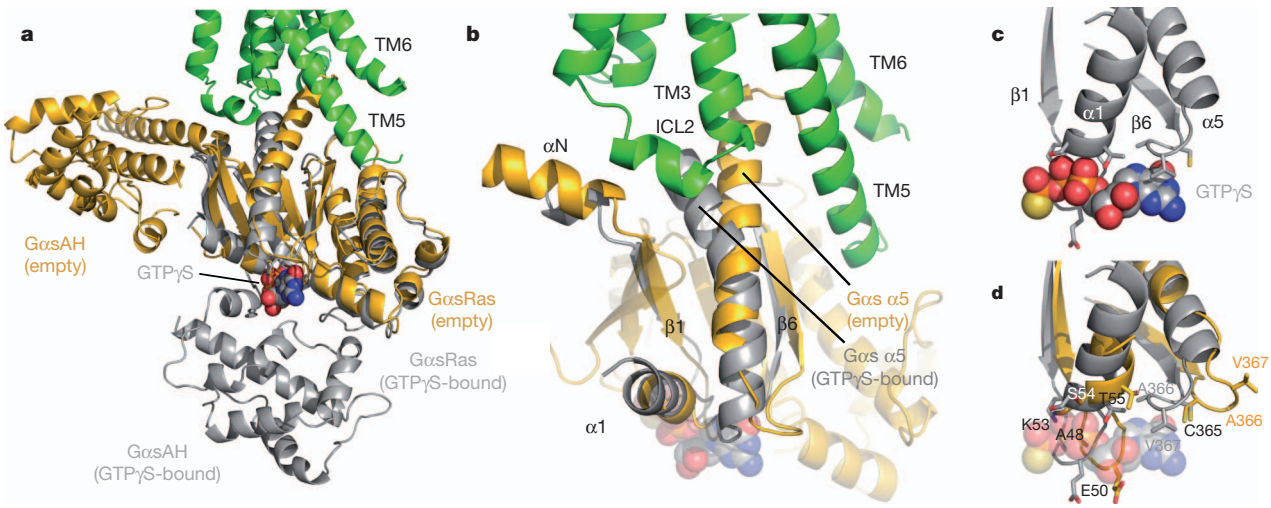

Figure 5 | Conformational changes in Gαs. **a**, A comparison of Gαs in the β_2AR–Gs complex (orange) with the GTPγS-bound Gαs (grey)[26] (PDB ID: 1AZT). GTPγS is shown as spheres. The helical domain of Gαs (GαsAH) shows a marked displacement relative to its position in the GTPγS-bound state. **b**, The α5-helix of Gαs is rotated and displaced towards the β_2AR, perturbing the β6-α5 loop, which otherwise forms part of the GTPγS-binding pocket. **c**, The β1-α1 loop (P-loop) and β6-α5 loop of Gαs interact with the phosphates and purine ring, respectively, of GTPγS in the Gαs–GTPγS structure. **d**, The β1-α1 and β6-α5 loops are rearranged in the nucleotide-free β_2AR–Gs structure.

Assembly of the β_2AR–Gs complex

Clues to the initial stages of complex formation may come from the recent active state structures of rhodopsin[32,33]. Figure 6a, b compares the active-state structure of β_2AR in the β_2AR–Gs complex with the recent structure of metarhodopsin II bound to a peptide representing the carboxy terminus of transducin[32]. The conformational changes in TM5 and TM6 are smaller in metarhodopsin II, and the position of the carboxy-terminal α helix of transducin is tilted by approximately 30° relative to the position of the homologous region of Gs. These may represent fundamental differences in the receptor–G protein interactions between these two proteins, but given the conservation of the G-protein binding pocket, the changes more probably reflect the more extensive contacts formed with the intact G protein. The position of the transducin peptide in metarhodopsin II may represent the initial interaction between a GDP-bound G protein and a GPCR. We have attempted to reproduce a similar complex between the β_2AR and a synthetic peptide representing the carboxy-terminal 20 amino acids of Gs, but did not observe any effect of this peptide on receptor function, possibly due to the solubility and behaviour of the peptide in solution. However, when the carboxy-terminal 20 amino acids of Gs are fused to the carboxy terminus of the β_2AR (Fig. 6c), we observe a 27-fold increase in agonist affinity (Fig. 6d). This effect is only 3.5-fold smaller than the effect we observe on agonist binding affinity in the β_2AR–Gs complex, and demonstrates that there is a functional interaction between the peptide and receptor that may represent an initial stage in β_2AR–Gs complex formation. Figure 6e and f presents a possible sequence of interactions of β_2AR and Gs when forming the nucleotide-free complex. The first interaction of the β_2AR with the Gs heterotrimer would require a movement of the carboxy terminus of the α5-helix away from the β6-strand to permit interactions with the β_2AR similar to those observed in metarhodopsin II (Fig. 6e). The availability of the carboxy terminus of the α5-helix for interactions with the β_2AR is supported by deuterium exchange studies[35] showing that this segment is more dynamic in the Gs-GDP heterotrimer than would be expected from the crystal structure of Gαs[26]. The subsequent formation of more extensive interactions between the β_2AR ICL2 and the amino terminus of Gαs requires a rotation of GαsRas relative to the receptor and would be associated with further conformational changes in both β_2AR and GαsRas (Fig. 6f). We cannot say when GDP is released during the formation of the complex; however, we speculate that uncoupling of the GαsAH from GαsRas is a consequence of nucleotide release or at least a coincident event. This binding model is in agreement with deuterium exchange experiments[35].

The β_2AR–Gs complex crystal structure provides the first high-resolution view of transmembrane signalling for a GPCR. We now have a framework to design experiments to investigate the mechanism of complex formation, GTP binding and complex dissociation. Of particular interest will be studies designed to determine the functional significance of the large movement of GαsAH relative to GαsRas that is observed in the β_2AR–Gs complex. A better understanding of the structural basis for G protein activation may provide new approaches for drug discovery. The high degree of structural homology within the ligand-binding pocket has posed challenges for developing highly selective drugs for specific GPCR targets. In contrast, there is relatively low homology at the interface between the β_2AR and Gαs, so identifying sequence and structural features that define specificity for particular G proteins may enable the development of selective inhibitors of specific GPCR–G protein interactions.

METHODS SUMMARY

The β_2AR–Gs complex was crystallized from β_2AR and Gs protein expressed in insect cells. Crystallogenesis was aided by fusing T4 lysozyme to the amino terminus of the β_2AR and the addition of a nanobody (Nb35) that binds at the interface between the Gα and Gβ subunits. Crystals were grown in a LCP using 7.7 MAG, a lipid that accommodates membrane proteins with larger hydrophilic surfaces[15]. Diffraction data were measured at beamline 23ID-B of the Advanced Photon Source and the structure was solved by molecular replacement. For more experimental details see Methods.

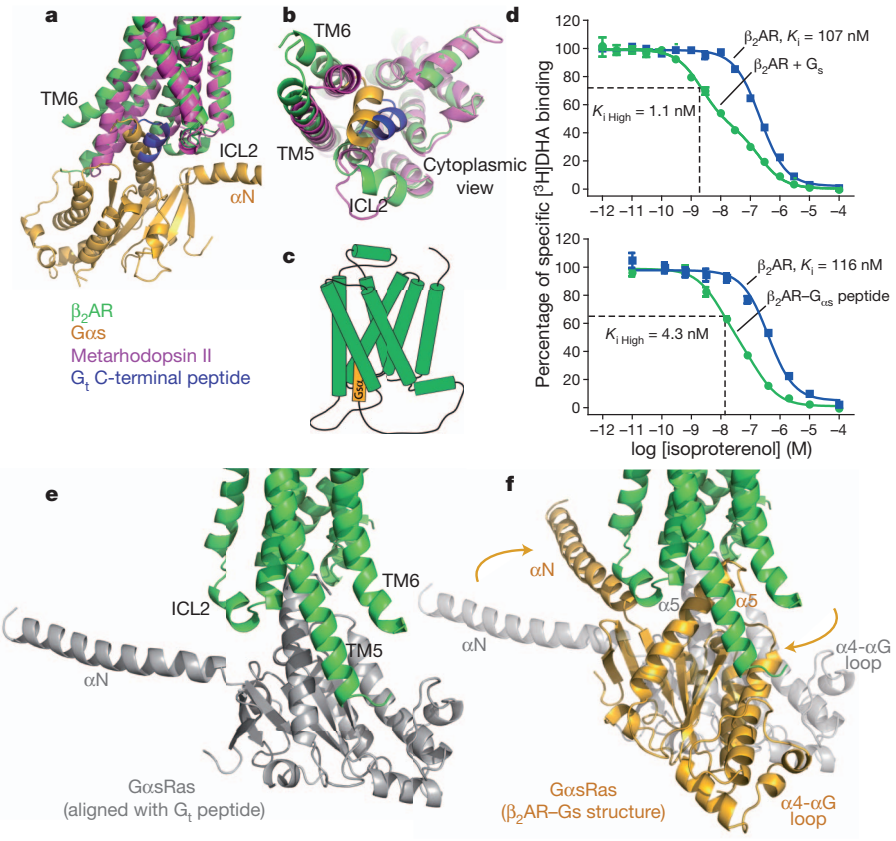

Figure 6 | Possible sequence of β_2AR–Gs complex formation. **a**, **b**, Comparison of the β_2AR–Gs structure (green and orange) with metarhodopsin II[32] (PDB ID: 3PQR) (purple) bound with the carboxy-terminal peptide of transducin (G_t) (blue). TM7 has been omitted in panel **a** to better visualize the G proteins. **c**, Cartoon of the β_2AR–Gαs peptide fusion construct used in the binding experiments (**d**). **d**, Competition binding experiments between [^{3}H]dihydroalprenolol ([^{3}H]DHA) and full agonist isoproterenol. Top panel shows binding data (reproduced from ref. 12) on β_2AR reconstituted in HDL particles with and without Gs heterotrimer. The fraction of β_2AR in the $K_{i\ High}$ state for the β_2AR with Gs is 0.55. Bottom panel shows binding to β_2AR and a β_2AR–Gαs peptide fusion expressed in *Sf*9 cell membranes. The fraction of β_2AR in the $K_{i\ High}$ state for the β_2AR–Gαs peptide fusion is 0.68. **e**, The initial interaction of agonist-bound β_2AR and GαsRas may involve an orientation of the carboxy terminus of GαsRas similar to that of the carboxy-terminal peptide of transducin in the structure of metarhodopsin II. **f**, The final position of GαsRas on the β_2AR as observed in the β_2AR–Gs complex.

Full Methods and any associated references are available in the online version of the paper at www.nature.com/nature.

Received 8 June; accepted 11 July 2011.
Published online 19 July 2011.

1. Dixon, R. A. *et al.* Cloning of the gene and cDNA for mammalian β-adrenergic receptor and homology with rhodopsin. *Nature* **321,** 75–79 (1986).
2. Rasmussen, S. G. *et al.* Crystal structure of the human β_2 adrenergic G-protein-coupled receptor. *Nature* **450,** 383–387 (2007).
3. Rosenbaum, D. M. *et al.* GPCR engineering yields high-resolution structural insights into β_2-adrenergic receptor function. *Science* **318,** 1266–1273 (2007).
4. Lefkowitz, R. J. Seven transmembrane receptors: something old, something new. *Acta Physiol. (Oxf.)* **190,** 9–19 (2007).
5. Brandt, D. R., Asano, T., Pedersen, S. E. & Ross, E. M. Reconstitution of catecholamine-stimulated guanosinetriphosphatase activity. *Biochemistry* **22,** 4357–4362 (1983).
6. Cerione, R. A. *et al.* The mammalian β_2-adrenergic receptor: reconstitution of functional interactions between pure receptor and pure stimulatory nucleotide binding protein of the adenylate cyclase system. *Biochemistry* **23,** 4519–4525 (1984).
7. Ross, E. M., Maguire, M. E., Sturgill, T. W., Biltonen, R. L. & Gilman, A. G. Relationship between the β-adrenergic receptor and adenylate cyclase. Studies of ligand binding and enzyme activity in purified membranes of S49 lymphoma cells. *J. Biol. Chem.* **252,** 5761–5775 (1977).
8. De Lean, A., Stadel, J. M. & Lefkowitz, R. J. A ternary complex model explains the agonist-specific binding properties of the adenylate cyclase-coupled β-adrenergic receptor. *J. Biol. Chem.* **255,** 7108–7117 (1980).
9. Fredriksson, R., Lagerstrom, M. C., Lundin, L. G. & Schioth, H. B. The G-protein-coupled receptors in the human genome form five main families. Phylogenetic analysis, paralogon groups, and fingerprints. *Mol. Pharmacol.* **63,** 1256–1272 (2003).
10. Azzi, M. *et al.* β-arrestin-mediated activation of MAPK by inverse agonists reveals distinct active conformations for G protein-coupled receptors. *Proc. Natl Acad. Sci. USA* **100,** 11406–11411 (2003).
11. Lefkowitz, R. J. & Shenoy, S. K. Transduction of receptor signals by β-arrestins. *Science* **308,** 512–517 (2005).
12. Rasmussen, S. G. *et al.* Structure of a nanobody-stabilized active state of the β_2 adrenoceptor. *Nature* **469,** 175–180 (2011).
13. Chae, P. S. *et al.* Maltose-neopentyl glycol (MNG) amphiphiles for solubilization, stabilization and crystallization of membrane proteins. *Nature Methods* **7,** 1003–1008 (2010).
14. Sprang, S. R. G protein mechanisms: insights from structural analysis. *Annu. Rev. Biochem.* **66,** 639–678 (1997).
15. Misquitta, L. V. *et al.* Membrane protein crystallization in lipidic mesophases with tailored bilayers. *Structure* **12,** 2113–2124 (2004).
16. Domanska, K. *et al.* Atomic structure of a nanobody-trapped domain-swapped dimer of an amyloidogenic β2-microglobulin variant. *Proc. Natl Acad. Sci. USA* **108,** 1314–1319 (2011).
17. Warne, T. *et al.* Structure of a β_1-adrenergic G-protein-coupled receptor. *Nature* **454,** 486–491 (2008).
18. Hofmann, K. P. *et al.* A G protein-coupled receptor at work: the rhodopsin model. *Trends Biochem. Sci.* **34,** 540–552 (2009).
19. Moro, O., Lameh, J., Hogger, P. & Sadee, W. Hydrophobic amino acid in the i2 loop plays a key role in receptor-G protein coupling. *J. Biol. Chem.* **268,** 22273–22276 (1993).
20. Baltensperger, K. *et al.* The β-adrenergic receptor is a substrate for the insulin receptor tyrosine kinase. *J. Biol. Chem.* **271,** 1061–1064 (1996).
21. Jastrzebska, B., Tsybovsky, Y. & Palczewski, K. Complexes between photoactivated rhodopsin and transducin: progress and questions. *Biochem. J.* **428,** 1–10 (2010).
22. Johnston, C. A. & Siderovski, D. P. Receptor-mediated activation of heterotrimeric G-proteins: current structural insights. *Mol. Pharmacol.* **72,** 219–230 (2007).
23. Breitwieser, G. E. G protein-coupled receptor oligomerization: implications for G protein activation and cell signaling. *Circ. Res.* **94,** 17–27 (2004).
24. Banères, J. L. & Parello, J. Structure-based analysis of GPCR function: evidence for a novel pentameric assembly between the dimeric leukotriene B4 receptor BLT1 and the G-protein. *J. Mol. Biol.* **329,** 815–829 (2003).
25. Angers, S., Salahpour, A. & Bouvier, M. Dimerization: an emerging concept for G protein-coupled receptor ontogeny and function. *Annu. Rev. Pharmacol. Toxicol.* **42,** 409–435 (2002).
26. Sunahara, R. K., Tesmer, J. J., Gilman, A. G. & Sprang, S. R. Crystal structure of the adenylyl cyclase activator $G_{s\alpha}$. *Science* **278,** 1943–1947 (1997).
27. Van Eps, N. *et al.* Interaction of a G protein with an activated receptor opens the interdomain interface in the α subunit. *Proc. Natl Acad. Sci. USA* **108,** 9420–9424 (2011).
28. Markby, D. W., Onrust, R. & Bourne, H. R. Separate GTP binding and GTPase activating domains of a Gα subunit. *Science* **262,** 1895–1901 (1993).
29. Conklin, B. R. & Bourne, H. R. Structural elements of Gα subunits that interact with Gβγ, receptors, and effectors. *Cell* **73,** 631–641 (1993).
30. Oldham, W. M. & Hamm, H. E. Heterotrimeric G protein activation by G-protein-coupled receptors. *Nature Rev. Mol. Cell Biol.* **9,** 60–71 (2008).
31. Wall, M. A. *et al.* The structure of the G protein heterotrimer $G_{i\alpha1}\beta_1\gamma_2$. *Cell* **83,** 1047–1058 (1995).
32. Choe, H. W. *et al.* Crystal structure of metarhodopsin II. *Nature* **471,** 651–655 (2011).
33. Standfuss, J. *et al.* The structural basis of agonist-induced activation in constitutively active rhodopsin. *Nature* **471,** 656–660 (2011).
34. Westfield, G. *et al.* Structurall flexibility of the Gαs α-helical domain in the β2-adrenoceptor Gs complex. *Proc. Nati Acad. Sci. USA* doi:10.1073/pnas.1113645108 (in the press).
35. Chung, K. Y. *et al.* β2 adrenergic receptor-induced conformational changes in the heterotrimeric G protein Gs. *Nature* doi:10.1038/nature10488 (this issue).

Supplementary Information is linked to the online version of the paper at www.nature.com/nature.

Acknowledgements We acknowledge support from National Institutes of Health Grants NS028471 (B.K.K.) and GM083118 (B.K.K. and R.K.S.), GM56169 (W.I.W.), P01 GM75913 (S.H.G), T32-GM008270 and P60DK-20572 (R.K.S.), GM75915, P50GM073210 and U54GM094599 (M.C.), Science Foundation Ireland (07/IN.1/B1836) and FP7 COST Action CM0902 (M.C.),the Mathers Foundation (B.K.K. and W.I.W.), the Lundbeck Foundation (Junior Group Leader Fellowship, S.G.F.R.), the University of Michigan Biomedical Sciences Scholars Program (R.K.S.), the Fund for Scientific Research of Flanders (FWO-Vlaanderen) and the Institute for the encouragement of Scientific Research and Innovation of Brussels (ISRIB) (E.P. and J.S.), The Danish Council for Independent Research, Medical Sciences (J.M.M.). We thank D. Grayson and A. Coughlan for help with lipid synthesis.

Author Contributions S.G.F.R. performed the final stages of β_2AR purification; assisted with β_2AR and Gs protein virus production and expression in insect cell cultures; worked out conditions to form and stabilize the β_2AR–Gs complex following screening, identification and characterization of the BI-167107 agonist and MNG-3 detergent; developed the β_2AR–Gs complex purification strategy with B.K.K. and characterized the stability of the complex under a variety of conditions; purified and analysed all preparations of the β_2AR–Gs complex used for crystallography, DXMS and electron microscopy studies, immunization, and nanobody selection; expressed and purified nanobodies and characterized β_2AR–Gs–Nb binding by size exclusion chromatography; set up crystallization trials in detergent solution, bicelles and lipidic cubic phase; crystallized the T4L–β_2AR–Gs, T4L–β_2AR–Gs–Nb37 and T4L–β_2AR–Gs–Nb35 complexes; optimized crystallization conditions and grew crystals for data collection; assisted with data collection and manuscript preparation. B.T.D. managed Gs heterotrimer subunit virus production and titration; expressed and purified Gs protein; with R.K.S. he identified the use of apyrase in forming the β_2AR–Gs complex and foscarnet/pyrophosphate during crystallogenesis; reconstituted the β_2AR–Gs complex and receptor alone in high density lipoprotein particles which were used for the initial nanobody selection. He assisted with data collection. Y.Z. designed, generated and optimized the T4L–β_2AR fusion protein, characterized its expression and functional properties, and prepared baculovirus for large scale expression. A.C.K. collected crystals, collected and processed diffraction data, solved and refined the structure, and assisted with manuscript preparation. K.Y.C. developed the cross-linking conditions for the purified β_2AR–Gs complex used for immunization of llamas. E.P. performed llama immunization, cloned and expressed nanobodies and performed initial selections. J.S. supervised nanobody production. D.C. assisted with Gs heterotrimer expression and purification. J.M.M. generated the β_2AR–Gsα peptide fusion construct, expressed it in insect cell membranes and performed competition binding experiments. F.S.T. expressed β_2AR in insect cell cultures and with T.S.K. performed the initial stage of β_2AR purification. S.T.A.S., J.A.L. and M.C. provided the 7.7 MAG lipid and helpful suggestions for lipidic mesophase crystallization using this lipid. P.S.C. and S.H.G. provided MNG-3 detergent for stabilization of the β_2AR–Gs complex. G.S. provided the essential feedback from the electron microscopy studies that helped guide the crystallization effort. W.I.W. oversaw data processing, structure determination and refinement. R.K.S. supervised Gs protein production, provided valuable ideas and insights into Gs structure and function, and assisted with data collection and manuscript preparation. B.K.K. was responsible for overall project strategy and management, harvested crystals and assisted with collection of diffraction data, and wrote the manuscript.

Author Information Coordinates and structure factors for the β_2AR–Gs complex are deposited in the Protein Data Bank (accession code 3SN6). Reprints and permissions information is available at www.nature.com/reprints. The authors declare no competing financial interests. Readers are welcome to comment on the online version of this article at www.nature.com/nature. Correspondence and requests for materials should be addressed to B.K.K. (kobilka@stanford.edu) or R.K.S. (sunahara@umich.edu).

METHODS

Expression and purification of β_2AR, Gs heterotrimer and nanobody-35. An amino-terminally fused T4 lysozyme–β_2AR construct with β_2AR truncated in position 365 (T4L–β_2AR, described in detail below) was expressed in *Sf*9 insect cell cultures infected with recombinant baculovirus (BestBac, Expression Systems), and solubilized in *n*-dodecyl-β-D-maltoside (DDM) according to methods described previously[36] (see Supplementary Fig. 7 for purification overview). A β_2AR construct truncated after residue 365 (β_2AR-365) was used for the majority of the analytical experiments. M1 Flag affinity chromatography (Sigma) served as the initial purification step followed by alprenolol-Sepharose chromatography for selection of functional receptor. A subsequent M1 Flag affinity chromatography step was used to exchange receptor-bound alprenolol for high-affinity agonist BI-167107. The agonist-bound receptor was eluted, dialysed against buffer (20 mM HEPES, pH 7.5, 100 mM NaCl, 0.1% DDM and 10 μM BI-167107), treated with lambda phosphatase (New England Biolabs), and concentrated to approximately 50 mg ml^{-1} with a 50 kDa molecular weight cut off (MWCO) Millipore concentrator. Prior to spin concentration, the β_2AR-365 construct, but not T4L–β_2AR, was treated with PNGaseF (New England Biolabs) to remove amino-terminal amino-linked glycosylation. The purified receptor was routinely analysed by SDS–PAGE/Coomassie brilliant blue staining (see Supplementary Fig. 8a).

Bovine Gαs short, His_6-rat $G\beta_1$ and bovine $G\gamma_2$ were expressed in HighFive insect cells (Invitrogen) grown in Insect Xpress serum-free media (Lonza). Cultures were grown to a density of 1.5 million cells per ml and then infected with three separate *Autographa californica* nuclear polyhedrosis viruses each containing the gene for one of the G protein subunits at a 1:1 multiplicity of infection (the viruses were a gift from A. Gilman). After 40–48 h of incubation the infected cells were harvested by centrifugation and resuspended in 75 ml lysis buffer (50 mM HEPES, pH 8.0, 65 mM NaCl, 1.1 mM $MgCl_2$, 1 mM EDTA, 1× PTT (35 μg ml^{-1} phenylmethanesulphonyl fluoride, 32 μg ml^{-1} tosyl phenylalanyl chloromethyl ketone, 32 μg ml^{-1} tosyl lysyl chloromethyl ketone), 1× LS (3.2 μg ml^{-1} leupeptin and 3.2 μg ml^{-1} soybean trypsin inhibitor), 5 mM β-mercaptoethanol (β-ME), and 10 μM GDP) per litre of culture volume. The suspension was pressurized with 600 p.s.i. N_2 for 40 min in a nitrogen cavitation bomb (Parr Instrument Company). After depressurization, the lysate was centrifuged to remove nuclei and unlysed cells, and then ultracentrifuged at 180,000*g* for 40 min. The pelleted membranes were resuspended in 30 ml wash buffer (50 mM HEPES, pH 8.0, 50 mM NaCl, 100 μM $MgCl_2$, 1× PTT, 1× LS, 5 mM β-ME, 10 μM GDP) per litre culture volume using a Dounce homogenizer and centrifuged again at 180,000*g* for 40 min. The washed pellet was resuspended in a minimal volume of wash buffer and flash-frozen with liquid nitrogen.

The frozen membranes were thawed and diluted to a total protein concentration of 5 mg ml^{-1} with fresh wash buffer. Sodium cholate detergent was added to the suspension at a final concentration of 1.0%, $MgCl_2$ was added to a final concentration of 5 mM, and 0.05 mg of purified protein phosphatase 5 (prepared in house) was added per litre of culture volume. The sample was stirred on ice for 40 min, and then centrifuged at 180,000*g* for 40 min to remove insoluble debris. The supernatant was diluted fivefold with Ni-NTA load buffer (20 mM HEPES, pH 8.0, 363 mM NaCl, 1.25 mM $MgCl_2$, 6.25 mM imidazole, 0.2% Anzergent 3-12, 1× PTT, 1× LS, 5 mM β-ME, 10 μM GDP), taking care to add the buffer slowly to avoid dropping the cholate concentration below its critical micelle concentration too quickly. Ni-NTA resin (3 ml; Qiagen) pre-equilibrated in Ni-NTA wash buffer 1 (20 mM HEPES, pH 8.0, 300 mM NaCl, 2 mM $MgCl_2$, 5 mM imidazole, 0.2% cholate, 0.15% Anzergent 3-12, 1× PTT, 1× LS, 5 mM β-ME, 10 μM GDP) per litre culture volume was added and the sample was stirred on ice for 20 min. The resin was collected into a gravity column and washed with 4× column volumes of Ni-NTA wash buffer 1, Ni-NTA wash buffer 2 (20 mM HEPES, pH 8.0, 50 mM NaCl, 1 mM $MgCl_2$, 10 mM imidazole, 0.15% Anzergent 3-12, 0.1% DDM, 1× PTT, 1× LS, 5 mM β-ME, 10 μM GDP), and Ni-NTA wash buffer 3 (20 mM HEPES, pH 8.0, 50 mM NaCl, 1 mM $MgCl_2$, 5 mM imidazole, 0.1% DDM, 1× PTT, 1× LS, 5 mM β-ME, 10 μM GDP). The protein was eluted with Ni-NTA elution buffer (20 mM HEPES, pH 8.0, 40 mM NaCl, 1 mM $MgCl_2$, 200 mM imidazole, 0.1% DDM, 1× PTT, 1× LS, 5 mM β-ME, 10 μM GDP). Protein-containing fractions were pooled and $MnCl_2$ was added to a final concentration of 100 μM. Purified lambda protein phosphatase (50 μg; prepared in house) was added per litre of culture volume and the eluate was incubated on ice with stirring for 30 min. The eluate was passed through a 0.22-μm filter and loaded directly onto a MonoQ HR 16/10 column (GE Healthcare) equilibrated in MonoQ buffer A (20 mM HEPES, pH 8.0, 50 mM NaCl, 100 μM $MgCl_2$, 0.1% DDM, 5 mM β-ME, 1× PTT). The column was washed with 150 ml buffer A at 5 ml min^{-1} and bound proteins were eluted over 350 ml with a linear gradient up to 28% MonoQ buffer B (same as buffer A except with 1 M NaCl). Fractions were collected in tubes spotted with enough GDP to make a final concentration of 10 μM. The Gs-containing fractions were concentrated to 2 ml using a stirred ultrafiltration cell (Amicon) with a 10-kDa nominal molecular weight limit (NMWL) regenerated cellulose membrane (Millipore). The concentrated sample was run on a Superdex 200 prep grade XK 16/70 column (GE Healthcare) equilibrated in S200 buffer (20 mM HEPES, pH 8.0, 100 mM NaCl, 1.1 mM $MgCl_2$, 1 mM EDTA, 0.012% DDM, 100 μM TCEP, 2 μM GDP). The fractions containing pure Gs were pooled, glycerol was added to 10% final concentration, and then the protein was concentrated to at least 10 mg ml^{-1} using a 30 kDa MWCO centrifugal ultrafiltration device (Millipore). The concentrated sample was then aliquoted, flash frozen, and stored at −80 °C. A typical yield of final, purified Gs heterotrimer from 8 l of cell culture volume was 6 mg.

Nanobody-35 (Nb35) was expressed in the periplasm of *E. coli* strain WK6, extracted, and purified by nickel affinity chromatography according to previously described methods[12] followed by ion-exchange chromatography (Supplementary Fig. 9a) using a Mono S 10/100 GL column (GE Healthcare). Selected Nb35 fractions were dialysed against buffer (10 mM HEPES, pH 7.5, 100 mM NaCl) and concentrated to approximately 65 mg ml^{-1} with a 10 kDa MWCO Millipore concentrator.

Complex formation, stabilization and purification. Formation of a stable complex (see Supplementary Fig. 10) was accomplished by mixing Gs heterotrimer at approximately 100 μM concentration with BI-167107-bound T4L–β_2AR (or β_2AR-365) in molar excess (approximately 130 μM) in 2 ml buffer (10 mM HEPES, pH 7.5, 100 mM NaCl, 0.1% DDM, 1 mM EDTA, 3 mM $MgCl_2$, 10 μM BI-167107) and incubating for 3 h at room temperature. BI-167107, which was identified from screening and characterizing approximately 50 different β_2AR agonists (data not shown), has a dissociation half-time of approximately 30 h, providing a higher degree of stabilization to the active G protein-bound receptor than other full agonists such as isoproterenol[12]. To maintain the high-affinity nucleotide-free state of the complex, apyrase (25 mU ml^{-1}, NEB) was added after 90 min to hydrolyse residual GDP released from Gαs upon binding to the receptor. GMP resulting from hydrolysis of GDP by apyrase has very poor affinity for the G protein in the complex. Rebinding of GDP can cause dissociation of the β_2AR–Gs complex (Supplementary Fig. 1a).

The β_2AR–Gs complex in DDM shows significant dissociation after 48 h at 4 °C (Supplementary Fig. 11a). We screened and characterized over 50 amphiphiles (data not shown) and identified MNG-3 (refs 12, 13; NG-310, Affymetrix-Anatrace) and its closely related analogues as detergents that substantially stabilize the complex (Supplementary Fig. 11a). The complex was exchanged into MNG-3 by adding the β_2AR–Gs mixture (2 ml) to 8 ml buffer (20 mM HEPES, pH 7.5, 100 mM NaCl, 10 μM BI-167107) containing 1% MNG-3 for 1 h at room temperature.

At this stage the mixture contains the β_2AR–Gs complex, non-functional Gs, and an excess of β_2AR. To separate functional β_2AR–Gs complex from non-functional Gs, and to complete the detergent exchange, the β_2AR–Gs complex was immobilized on M1 Flag resin and washed in buffer (20 mM HEPES, pH 7.5, 100 mM NaCl, 10 μM BI-167107, and 3 mM $CaCl_2$) containing 0.2% MNG-3. To prevent cysteine bridge-mediated aggregation of β_2AR–Gs complexes, 100 μM TCEP was added to the eluted protein before concentrating it with a 50 kDa MWCO Millipore concentrator. Of note, it was discovered later that crystal growth improved at even higher TCEP concentrations (above 1 mM) compared to 100 μM TCEP, and that the integrity of the β_2AR–Gs complex in MNG-3 was stable to 10 mM TCEP as measured by gel filtration analysis (Supplementary Fig. 12). In contrast, DDM-solubilized β_2AR loses its ability to bind the high-affinity antagonist [^{3}H]dihydroalprenolol ([^{3}H]DHA) in 10 mM TCEP (data not shown), probably due to disruption of extracellular disulphide bonds. Iodoacetamide could not be used to block reactive cysteines on Gs α and β subunits as it caused dissociation of the β_2AR–Gs complex (Supplementary Fig. 12b). The final size exclusion chromatography procedure to separate excess free receptor from the β_2AR–Gs complex (Supplementary Fig. 8b) was performed on a Superdex 200 10/300 GL column (GE Healthcare) equilibrated with buffer containing 0.02% MNG-3, 10 mM HEPES, pH 7.5, 100 mM NaCl, 10 μM BI-167107 and 100 μM TCEP. Peak fractions were pooled (Supplementary Fig. 8b) and concentrated to approximately 90 mg ml^{-1} with a 100 kDa MWCO Viva-spin concentrator and analysed by SDS–PAGE/Coomassie brilliant blue staining (Supplementary Fig. 8a) and gel filtration (Supplementary Fig. 8c). To confirm a pure, homogeneous and dephosphorylated preparation, the β_2AR–Gs complex was routinely analysed by ion exchange chromatography (Supplementary Fig. 8d).

Protein engineering. To increase the probability of obtaining crystals of the β_2AR–Gs complex we set out to increase the polar surface area on the extracellular side of the receptor using two strategies. The first approach, to generate extracellular binding antibodies, was not successful. The second approach was to replace the flexible and presumably unstructured amino terminus with the globular protein T4 lysozyme (T4L) used previously to crystallize and solve the carazolol-bound receptor[3] The construct used here (T4L–β_2AR) contained the

cleavable signal sequence followed by the M1 Flag epitope (DYKDDDDA), the Tobacco etch virus (TEV) protease recognition sequence (ENLYFQG), bacteriophage T4 lysozyme from N2 through Y161 including C54T and C97A mutations, and a two residue alanine linker fused to the human β_2AR sequence D29 through G365. The PNGaseF-inaccessible glycosylation site of the β_2AR at N187 was mutated to Glu. M96 and M98 in the first extracellular loop were each replaced by Thr to increase the otherwise low expression level of T4L–β_2AR. The threonine mutations did not affect ligand binding affinity for [^{3}H]DHA, but caused a small, approximately twofold decrease in affinity for isoproterenol (data not shown).

The β_2AR–Gs peptide fusion construct used for [^{3}H]DHA competition binding with isoproterenol was constructed from the receptor truncated at position 365 and fused to the last 21 amino acids of the Gαs subunit (amino acids 374–394, except for C379A). A Gly-Ser is inserted between the receptor and the peptide. Also an extended TEV protease site (**SENLYFQG**S) was introduced in the β_2AR between G360 and G361.

Stabilization of Gs with nanobodies. From negative stain electron microscopy imaging[34], we observed that the α-helical domain of Gαs was flexible and therefore possibly responsible for poor crystal quality. Targeted stabilization of this domain was addressed by immunizing two llamas (*Lama glama*) with the bis(sulphosuccinimidyl)glutarate (BS2G, Pierce) cross-linked β_2AR–Gs-BI-167107 ternary complex. Peripheral blood lymphocytes were isolated from the immunized animals to extract total RNA, prepare cDNA and construct a Nanobody phage display library according to published methods[16]. Nb35 and Nb37 were enriched by two rounds of biopanning on the β_2AR–Gs-BI-167107 ternary complex embedded in biotinylated high-density lipoprotein particles[37]. Nb35 and Nb37 were selected for further characterization because they bind the β_2AR–Gs-BI-167107 ternary complex but not the free receptor in an ELISA assay. Nanobody binding to the β_2AR–Gs complex was confirmed by size exclusion chromatography (Supplementary Fig. 1d), and it was noted that both nanobodies protected the complex from dissociation by GTPγS, suggestive of a stabilizing Gs–Nb interaction (Supplementary Fig. 1d).

Crystallization. BI-167107 bound T4L–β_2AR–Gs complex and Nb35 were mixed in 1:1.2 molar ratio. The small molar excess of Nb35 was verified by analytical gel filtration (see Supplementary Fig. 9b). The mixture incubated for 1 h at room temperature before mixing with 7.7 MAG (provided by M. Caffrey) containing 10% cholesterol (C8667, Sigma) in 1:1 protein solution to lipid ratio (w/w) using the twin-syringe mixing method reported previously[38]. The concentration of T4L–β_2AR–Gs–Nb35 complex in 7.7 MAG was approximately 25 mg ml^{-1}. We believe the detergent MNG-3 stabilizes the T4L–β_2AR–Gs complex during its incorporation into the lipid cubic phase. This may be due to the high affinity of MNG-3 for the receptor. The β_2AR in MNG-3 maintains its structural integrity even when diluted below the CMC of the detergent, in contrast to β_2AR in DDM, which rapidly loses binding activity (Supplementary Fig. 11b). Moreover, MNG-3 improved crystal size and quality, as previously reported[12,13,39]. The protein:lipid mixture was delivered through an LCP dispensing robot (Gryphon, Art Robbins Instruments) in 40 nl drops to either 24-well or 96-well glass sandwich plates and overlaid en-bloc with 0.8 µl precipitant solution. Multiple crystallization leads were initially identified using in-house screens partly based on reagents from the StockOptions Salt kit (Hampton Research). Crystals for data collection were grown in 18 to 22% PEG 400, 100 mM MES, pH 6.5 (Supplementary Fig. 1c), 350 to 450 mM potassium nitrate, 10 mM foscarnet (Supplementary Fig. 1b), 1 mM TCEP (Supplementary Fig. 12c), and 10 µM BI-167107. Crystals reached full size within 3–4 days at 20 °C and were picked from a sponge-like mesophase and flash-frozen in liquid nitrogen without additional cryoprotectant.

Microcrystallography data collection and processing. Diffraction data were measured at the Advanced Photon Source beamline 23 ID-B. Hundreds of crystals were screened, and a final data set was compiled using diffraction wedges of typically 10 degrees from 20 strongly diffracting crystals (Supplementary Table 2). All data reduction was performed using HKL2000 (ref. 40). Although in many cases diffraction to beyond 3 Å was seen in initial frames, radiation damage and anisotropic diffraction resulted in low completeness in higher resolution shells. Analysis of the final data set by the UCLA diffraction anisotropy server[41] indicated that diffraction along the a^* axis was superior to that in other directions. On the basis of an $F/\sigma(F)$ cutoff of 3 along each reciprocal space axis, reflections were subjected to an anisotropic truncation with resolution limits of 2.9, 3.2 and 3.2 Å along a^*, b^* and c^* before use in refinement. We report this structure to an overall resolution of 3.2 Å. Despite the low completeness in the highest resolution shells (Supplementary Table 3) inclusion of these reflections gave substantial improvements in map quality and lower R_{free} during refinement.

Structure solution and refinement. The structure was solved by molecular replacement using Phaser[42,43]. The order of the molecular replacement search was found to be critical in solving the structure. In order, the search models used were: the β and γ subunits from a Gi heterotrimer (PDB ID: 1GP2), the Gs α Ras-like domain (PDB ID: 1AZT), the active-state β_2AR (PDB ID: 3P0G), a β_2AR-binding nanobody (PDB ID: 3P0G), T4 lysozyme (PDB ID: 2RH1), and the Gs α-helical domain (PDB ID: 1AZT). Following the determination of the initial structure by molecular replacement, rigid body refinement and simulated annealing were performed in Phenix[44] and BUSTER[45], followed by restrained refinement and manual rebuilding in Coot[46]. After iterative refinement and manual adjustments, the structure was refined in CNS using the DEN method[47]. Although the resolution of this structure exceeds that for which DEN is typically most useful, the presence of several poorly resolved regions indicated that the incorporation of additional information to guide refinement could provide better results. The DEN reference models used were those used for molecular replacement, with the exception of NB35, which was well ordered and for which no higher resolution structure is available. Side chains were omitted from 53 residues for which there was no electron density past Cβ below a low contour level of 0.7σ in a $2Fo - Fc$ map. Figures were prepared using PyMOL (The PyMOL Molecular Graphics System, Version 1.3, Schrödinger, LLC.). MolProbity was used to determine Ramachandran statistics[48].

Competition binding. Membranes expressing the β_2AR or the β_2AR–Gs peptide fusion were prepared from baculovirus-infected *Sf*9 cells and [^{3}H]DHA-binding performed as previously described[49]. For competition binding, membranes were incubated with [^{3}H]DHA (1.1 nM final) and increasing concentrations of (−)-isoproterenol for 1 h before harvesting onto GF/B filters. Competition data were fitted to a two-site binding model and isoproterenol high and low K_i values and fractions calculated using GraphPad prism.

36. Kobilka, B. K. Amino and carboxyl terminal modifications to facilitate the production and purification of a G protein-coupled receptor. *Anal. Biochem.* **231,** 269–271 (1995).
37. Whorton, M. R. *et al.* A monomeric G protein-coupled receptor isolated in a high-density lipoprotein particle efficiently activates its G protein. *Proc. Natl Acad. Sci. USA* **104,** 7682–7687 (2007).
38. Caffrey, M. & Cherezov, V. Crystallizing membrane proteins using lipidic mesophases. *Nature Protocols* **4,** 706–731 (2009).
39. Rosenbaum, D. M. *et al.* Structure and function of an irreversible agonist-β_2 adrenoceptor complex. *Nature* **469,** 236–240 (2011).
40. Otwinowski, Z. & Minor, W. Processing of X-ray diffraction data collected in oscillation mode. *Methods Enzymol.* **276,** 307–326 (1997).
41. Strong, M. *et al.* Toward the structural genomics of complexes: crystal structure of a PE/PPE protein complex from *Mycobacterium tuberculosis*. *Proc. Natl Acad. Sci. USA* **103,** 8060–8065 (2006).
42. McCoy, A. J. Solving structures of protein complexes by molecular replacement with *Phaser*. *Acta Crystallogr. D* **63,** 32–41 (2007).
43. McCoy, A. J. *et al. Phaser* crystallographic software. *J. Appl. Cryst.* **40,** 658–674 (2007).
44. Afonine, P. V., Grosse-Kunstleve, R. W. & Adams, P. D. A robust bulk-solvent correction and anisotropic scaling procedure. *Acta Crystallogr. D* **61,** 850–855 (2005).
45. Blanc, E. *et al.* Refinement of severely incomplete structures with maximum likelihood in *BUSTER-TNT*. *Acta Crystallogr. D* **60,** 2210–2221 (2004).
46. Emsley, P. & Cowtan, K. *Coot*: model-building tools for molecular graphics. *Acta Crystallogr. D* **60,** 2126–2132 (2004).
47. Schröder, G. F., Levitt, M. & Brunger, A. T. Super-resolution biomolecular crystallography with low-resolution data. *Nature* **464,** 1218–1222 (2010).
48. Chen, V. B. *et al. MolProbity*: all-atom structure validation for macromolecular crystallography. *Acta Crystallogr. D* **66,** 12–21 (2010).
49. Swaminath, G., Steenhuis, J., Kobilka, B. & Lee, T. W. Allosteric modulation of β_2-adrenergic receptor by Zn^{2+}. *Mol. Pharmacol.* **61,** 65–72 (2002).